Electron states in rectangular quantum well wires (single wires, finite and infinite lattices)

E P Pokatilov†, V A Fonoberov†, S N Balaban†§ and V M Fomin‡‖

† Laboratory of Multilayer Structure Physics, Department of Theoretical Physics,
State University of Moldova, A. Mateevici 60, MD-2009 Chişinău, Moldova
‡ Theoretische Fysica van de Vaste Stof, Departement Natuurkunde,
Universiteit Antwerpen (UIA), Universiteitsplein 1, B-2610 Antwerpen, België

Abstract. Electron and hole states are studied in quantum well wires (QWWs) with a rectangular cross section. A theoretical approach is developed, within which the electronic properties of a single QWW as well as of finite and infinite planar lattices of QWWs are analysed. It is demonstrated that the ratio of effective masses in the well and in the barrier influences the dispersion law of the electron motion along the QWW axis. A six-wire lattice is studied in detail. Edge states, which can be observed in optical spectra, are revealed, when the barrier heights are different inside and outside the lattice. The miniband structure is investigated for an infinite lattice of QWWs. The evolution of electron states is analysed when the number of QWWs in the lattice increases: $1 \to 6 \to \infty$. The calculated electron–hole pair energies are in a good agreement with the experimental data on photoluminescence in the $Ga_{0.47}In_{0.53}As/InP$ QWW.

1. Introduction

Nowadays, the fabrication technology of semiconductor quantum well structures of nanometre sizes is being developed. These structures will form the basis of the electronic devices of the future. It has been proved that transistors and lasers made of quantum wires demonstrate excellent characteristics [1]. Among all of these structures, quantum well wires (QWWs) have attracted attention because of a combination of the confinement across a QWW and the free motion of a charge carrier along the QWW axis.

Recently, QWWs of various cross sectional shapes have been fabricated and their physical properties have been studied. QWWs with a triangular cross section have been obtained using the technology of the selective growth on SiO_2 patterned substrates [2]. Ultrafine Si/SiO_2 QWWs have been fabricated and their transport properties have been studied [3]. Cylindrical GaAs and CdSe QWWs have been formed in crysolite asbestos nanotubes and also the crystallization of CdS in the channels of mica has been carried out [4], where nonlinear optical transmission at discrete frequencies has been observed. The investigation of carrier capture, relaxation, cooling and radiative recombination in the V-groove $GaAs/Ga_{0.55}Al_{0.45}As$ QWW has been presented in [5]. The optical properties of the V-groove and T-shaped $GaAs/Al_xGa_{1-x}As$ QWWs have been investigated by observing photoluminescence (PL) and

§ Present address: Theoretische Fysica van de Vaste Stof, Departement Natuurkunde, Universiteit Antwerpen (UIA), Universiteitsplein 1, B-2610 Antwerpen, België.
‖ Permanent address: Laboratory of Multilayer Structure Physics, Department of Theoretical Physics, State University of Moldova, A. Mateevici 60, MD-2009 Chişinău, Moldova.
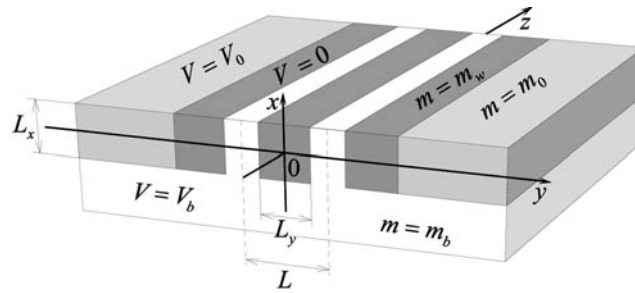
Figure 1. A schematic picture of a finite lattice. For instance, three quantum wires (dark grey), edge barrier (light grey) and barrier region (white) are shown. The structure is covered ($x > L_x/2$) by the same substance as its substrate ($x < -L_x/2$).

photoluminescence excitation (PLE) spectra, and the effect of lateral confinement on the valence-band mixing has been studied in [6, 7]. The mixing in the conduction band of V- and T-shaped QWWs has been studied in [8]. Strained V-shaped QWWs have been described in [9] by means of the eight-band $k \cdot p$ scheme. An impurity located at the axis of a cylindrical QWW has also been studied [10, 11]. The binding energy of a hydrogenic impurity in a cylindrical QWW has been calculated as a function of the location of the impurity with respect to the axis of the QWW [12]. The effect of the shape of a cross section on the impurity binding energies for a QWW has been investigated in [13]. A contribution of the polaron effect to the impurity binding energy in a cylindrical QWW has been analysed in [14].

Considerable theoretical and experimental attention is devoted to QWWs with a rectangular cross section. There is a simple cross-section anisotropy in these wires, which can be described by only one parameter (the ratio of the rectangle sides). It is also convenient to fabricate different lattices of such wires. Electron and hole states in GaAs/Ga$_{1-x}$Al$_x$As rectangular QWWs have been calculated in [15–17]. Magneto-phonon resonances [18] and magneto-plasmons and edge-spin-density modes [19] have been investigated in these QWWs using the simple parabolic potential well approximation. The binding energies of a hydrogenic impurity arbitrarily located in a rectangular QWW have been calculated in [20, 21]. The influence of the LO phonons confined to a rectangular QWW on the impurity ground-state energy has been considered in [22].

The first rectangular QWWs were made of Ga$_{0.47}$In$_{0.53}$As [23, 24] or GaAs [25] for the well and InP or Ga$_{0.63}$Al$_{0.37}$As, correspondingly, for the barrier. The height of the potential barrier for an electron in both cases was about 250 meV. A detailed investigation of optical properties of rectangular GaAs/AlAs QWWs has been carried out in [26] where the anisotropy of PL and PLE spectra has been studied. Lateral quantum confinement effects in the rectangular Ga$_{0.47}$In$_{0.53}$As/InP QWW have been examined [27] through PL experiments with and without magnetic field. Strain effects in the rectangular InAs$_{0.48}$P$_{0.52}$/InP QWW have been investigated in [28].

A few numerical methods have been suggested to solve the Schrödinger equation for QWWs with a rectangular cross section and with a finite height of the barrier potential. In [15] the eigenenergies in the rectangular GaAs/Ga$_{0.63}$Al$_{0.37}$As QWW have been calculated for an electron and a hole using the finite-element method. In [16] calculations have been carried out for the Ga$_{0.47}$In$_{0.53}$As/InP QWW expressing electron and hole wavefunctions in terms of a two-dimensional Fourier series. In [17], hole energy levels in the rectangular GaAs/Ga$_{0.8}$Al$_{0.2}$As QWW have been found using a variational method with the wavefunction written as a sum of Gaussians.

In order to find electron and hole quantum states in a system with an arbitrary number of rectangular QWWs, we develop a method, which includes a considerable analytical phase. In section 2 this method is applied for a single rectangular QWW and for a planar lattice with a finite number of rectangular QWWs. Further, in section 3 a planar lattice with an infinite number of QWWs is considered. The energy structure of an infinite lattice of QWWs is investigated. Results of calculations for a single QWW, a finite lattice with six QWWs, and an infinite lattice of QWWs are discussed in section 4. The obtained energy levels of an electron and a hole in a single QWW are compared with those obtained theoretically earlier [15, 16] and with experimental data [23, 24]. In a finite lattice of QWWs, we study in detail edge quantum states with the wavefunctions localized at the lattice ends. Conclusions about main features of the electron and hole quantum states in QWW lattices are given in section 5.

2. Single quantum wire and finite lattice

We consider the rectangular quantum wires layered out along one plane and parallel to each other (see figure 1). The dimensions of the quantum wires are L_x and L_y along the x-axis and the y-axis, respectively. The lengths of the quantum wires are supposed to be infinite. The wavefunctions and the energy spectrum of this structure are determined from the Schrödinger equation

$$-\frac{\hbar^2}{2}\nabla\left(\frac{1}{m(\boldsymbol{r})}\nabla\Psi(\boldsymbol{r})\right) + V(\boldsymbol{r})\Psi(\boldsymbol{r}) = E\Psi(\boldsymbol{r}) \tag{1}$$

where $m(\boldsymbol{r})$ and $V(\boldsymbol{r})$ are respectively the band mass and the barrier potential. Inside the quantum wires $V(\boldsymbol{r}) = 0$ and $m(\boldsymbol{r}) = m_w$. The height of the barrier potential and the band mass are chosen to be in general different outside the lattice ($V(\boldsymbol{r}) = V_0$, $m(\boldsymbol{r}) = m_0$) and in the spacings between the quantum wires ($V(\boldsymbol{r}) = V_b$, $m(\boldsymbol{r}) = m_b$).

Since $V(\boldsymbol{r})$ and $m(\boldsymbol{r})$ do not depend on z, we can represent $\Psi(\boldsymbol{r})$ in (1) as

$$\Psi(\boldsymbol{r}) = \exp(\mathrm{i}k_z z)\Psi(x, y) \tag{2}$$

i.e. a charge carrier travels freely along the z-axis with a wavenumber k_z. Substituting (2) in (1) gives the two-dimensional Schrödinger equation

$$-\frac{\hbar^2}{2}\nabla_2\left(\frac{1}{m(x, y)}\nabla_2\Psi(x, y)\right) + V^{\mathrm{eff}}(x, y)\Psi(x, y) = E^{\mathrm{tr}}\Psi(x, y) \tag{3}$$

where $E^{\mathrm{tr}} = E - \hbar^2 k_z^2/2m_w$ is referred to as the energy of the transverse (in the (x, y)-plane) motion and

$$V^{\mathrm{eff}}(x, y) = V(x, y) + \frac{\hbar^2 k_z^2}{2}\left(\frac{1}{m(x, y)} - \frac{1}{m_w}\right) \tag{4}$$

is the effective potential depending on k_z due to the inhomogeneity of the structure. We calculate the wavefunction $\Psi(x, y)$ separately in the region I ($|x| \leqslant L_x/2$) and in the region II ($|x| > L_x/2$). In each of these regions, the barrier potential and the band mass may be functions of variable y only:

$$V^{\mathrm{eff}}(x, y) \equiv V_{\mathrm{I}}(y) \qquad m(x, y) \equiv m(y) \qquad |x| \leqslant L_x/2$$
$$V^{\mathrm{eff}}(x, y) \equiv V_{\mathrm{II}} \qquad m(x, y) \equiv m_b \qquad |x| > L_x/2. \tag{5}$$

Consequently, we can use the following expansions for the wavefunction:

$$\Psi_{\mathrm{I}}(x, y) = \sum_k A_k \varphi_k(y) F_k(x), \tag{6}$$

$$\Psi_{\mathrm{II}}(x, y) = \sum_\kappa B_\kappa \Phi_\kappa(y) f_\kappa(x) \tag{7}$$

where Ψ_{I} and Ψ_{II} denote the wavefunction in regions I and II, respectively. It is worth noting that $V^{\text{eff}}(x, y)$ and $m(x, y)$ are symmetrical functions with respect to both the coordinates, i.e. they do not change when $x \rightarrow -x$ or $y \rightarrow -y$. Hence, a solution of (3) is either a symmetrical or antisymmetrical function of x and y. Hereafter, we introduce two indices i and j for the functions $F_k^i(x)$, $f_\kappa^i(x)$, $\varphi_k^j(y)$, $\Phi_\kappa^j(y)$ and for the coefficients A_k^{ij} and B_κ^{ij} to indicate the symmetry of the quantum state ($i, j = s$ for a symmetrical function and $i, j = a$ for a antisymmetrical one).

For further calculations it is convenient to impose an auxiliary condition on the wavefunction $\Psi(x, \pm R) = 0$, which, according to (6) and (7), results in the conditions $\varphi_k^j(\pm R) = 0$ and $\Phi_\kappa^j(\pm R) = 0$. The parameter R is chosen to be much larger than the size of the structure. We have found that for a GaAs/Ga$_{0.63}$Al$_{0.37}$As structure with N quantum wires, it is enough to take $2R = NL + 6L$ and a choice of higher values of R does not change the results of calculations considerably. If we assume, for example, $2R = NL + 7L$ then, even for energy levels that lie only $0.01V_b$ below the barrier edge, the corresponding energy differences are of the order of a few per cent.

The solution of (3) is divided into three steps. (i) We determine the functions $\varphi_k^j(y)$ and $\Phi_\kappa^j(y)$ with the corresponding quantum numbers k and κ. (ii) We find $F_k^i(x)$ and $f_\kappa^i(x)$. (iii) We require the continuity of the wavefunction $\Psi(x, y)$ and its derivative divided by the band mass at the boundary lines between the regions I and II ($|x| = L_x/2$), in order to obtain equations for the coefficients A_k^{ij} and B_κ^{ij} and a secular equation for the energy E^{tr}.

(i) Inserting the expansion (6) into (3), we find that terms depending on the x and y coordinates can be separated. Hence, equation (3) can be split into two parts, which correspond to one-dimensional equations for $F_k^i(x)$ and $\varphi_k^j(y)$. Thus, $\varphi_k^j(y)$ are the eigenfunctions of the one-dimensional equation

$$-\frac{\hbar^2}{2}\frac{\mathrm{d}}{\mathrm{d}y}\frac{1}{m(y)}\frac{\mathrm{d}\varphi_k^j(y)}{\mathrm{d}y} + \left(V_{\text{I}}(y) - E^{\text{tr}} + \frac{m_w}{m(y)}E^{\text{tr}}\right)\varphi_k^j(y) = \frac{\hbar^2 k^2}{2m(y)}\varphi_k^j(y). \tag{8}$$

The solution of this equation depends on the number of the quantum wires in the lattice. It can be solved analytically for an arbitrary number of QWWs in the lattice. Indeed, dividing the interval $(-R, R)$ into segments where the band mass is constant, one can easily find a solution of (8) in each of those segments. Then, satisfying the condition $\varphi_k^j(\pm R) = 0$ and requiring the continuity of the function $\varphi_k^j(y)$ and of its derivative divided by the band mass, one obtains a secular equation for quantum numbers k. We have considered two cases: a single QWW and a lattice with six QWWs. For a single quantum wire, the symmetrical solution is

$$\varphi_k^s(y) = \begin{cases} \cos(ky) & |y| \leqslant L_y/2 \\ \cos\left(k\dfrac{L_y}{2}\right)\dfrac{\sinh(q_k(R - |y|))}{\sinh(q_k(R - L_y/2))} & L_y/2 < |y| \leqslant R \end{cases} \tag{9}$$

where quantum numbers k are defined from the secular equation

$$q_k \coth(q_k(R - L_y/2)) = \frac{m_b}{m_w}k\tan(kL_y/2). \tag{10}$$

The antisymmetrical solution is

$$\varphi_k^a(y) = \begin{cases} \sin(ky) & |y| \leqslant L_y/2 \\ \text{sign}(y)\sin\left(k\dfrac{L_y}{2}\right)\dfrac{\sinh(q_k(R - |y|))}{\sinh(q_k(R - L_y/2))} & L_y/2 < |y| \leqslant R \end{cases} \tag{11}$$

with the corresponding secular equation

$$q_k \coth(q_k(R - L_y/2)) = -\frac{m_b}{m_w}k\cot(kL_y/2). \tag{12}$$

Here $q_k^2 = -k^2 + 2m_w E/\hbar^2 + 2m_b(V_b - E)/\hbar^2$, sign($t$) is the sign function. The parameter q_k can acquire either real or imaginary values.

Similarly, substituting the expansion (7) into (3), we obtain the one-dimensional equation for $\Phi_\kappa^j(y)$

$$-\frac{\hbar^2}{2m_b}\frac{\mathrm{d}^2\Phi_\kappa^j(y)}{\mathrm{d}y^2} - \frac{\hbar^2\kappa^2}{2m_b}\Phi_\kappa^j(y) = 0. \tag{13}$$

The solutions of this equation can be immediately written down as

$$\Phi_\kappa^s(y) = \frac{1}{\sqrt{R}}\cos(\kappa y) \qquad \Phi_\kappa^a(y) = \frac{1}{\sqrt{R}}\sin(\kappa y) \tag{14}$$

where the quantum number κ is found from the condition $\Phi_\kappa^j(\pm R) = 0$. The sets of eigenfunctions $\varphi_k^j(y)$ and $\Phi_\kappa^j(y)$ are complete. However, during our calculations we restrict the summation in the expansions (6) and (7) to a sufficient (in order to provide a given accuracy) number of terms, which is the same for both expansions.

(ii) Inserting expressions (6) and (7) into equation (3) again yields the one-dimensional equations for functions $F_k^i(x)$ and $f_\kappa^i(x)$:

$$-\frac{\hbar^2}{2m_w}\frac{\mathrm{d}^2 F_k^i(x)}{\mathrm{d}x^2} + \frac{\hbar^2 k^2}{2m_w}F_k^i(x) = E^{\mathrm{tr}}F_k^i(x) \tag{15}$$

$$-\frac{\hbar^2}{2m_b}\frac{\mathrm{d}^2 f_\kappa^i(x)}{\mathrm{d}x^2} + \frac{\hbar^2\kappa^2}{2m_b}f_\kappa^i(x) = (E^{\mathrm{tr}} - V_{\mathrm{II}})f_\kappa^i(x). \tag{16}$$

The general solutions of these equations are

$$F_k^s(x) = \theta\left(E^{\mathrm{tr}} - \frac{\hbar^2 k^2}{2m_w}\right)\cos(\nu_k x) + \theta\left(\frac{\hbar^2 k^2}{2m_w} - E^{\mathrm{tr}}\right)\cosh(\nu_k x)$$

$$F_k^a(x) = \theta\left(E^{\mathrm{tr}} - \frac{\hbar^2 k^2}{2m_w}\right)\sin(\nu_k x) + \theta\left(\frac{\hbar^2 k^2}{2m_w} - E^{\mathrm{tr}}\right)\sinh(\nu_k x) \tag{17}$$

$$f_\kappa^s(x) = \exp\left(\xi_\kappa\left(\frac{L_x}{2} - |x|\right)\right) \qquad f_\kappa^a(x) = \mathrm{sign}(x)\exp\left(\xi_\kappa\left(\frac{L_x}{2} - |x|\right)\right) \tag{18}$$

where

$$\nu_k = \sqrt{\left|-k^2 + \frac{2m_w E^{\mathrm{tr}}}{\hbar^2}\right|} \qquad \xi_\kappa = \sqrt{\kappa^2 + \frac{2m_b(V_{\mathrm{II}} - E^{\mathrm{tr}})}{\hbar^2}}$$

and $\theta(t)$ is the Heaviside step function. In (18), the requirement $f_\kappa(\pm\infty) = 0$ is fulfilled.

(iii) Since the wavefunction $\Psi(x, y)$ is either a symmetrical or an antisymmetrical function with respect to x, it is enough to require the continuity conditions for $\Psi(x, y)$ and for its derivative divided by the band mass at the boundary $x = L_x/2$. Using the fact that the functions $\Phi_\kappa^j(y)$ are orthonormalized, these boundary conditions result in

$$B_\kappa^{ij} = \sum_k d_{k\kappa}^j A_k^{ij} F_k^i(L_x/2) \qquad -\xi_\kappa B_\kappa^{ij} = -\sum_k D_{k\kappa}^j A_k^{ij} F_k^{i\,\prime}(L_x/2) \tag{19}$$

where $F_k^{i\,\prime}(x)$ is the derivative of the function $F_k^i(x)$, and

$$d_{k\kappa}^j = \int_{-R}^{R}\Phi_\kappa^j(y)\varphi_k^j(y)\,\mathrm{d}y \qquad D_{k\kappa}^j = \int_{-R}^{R}\frac{m_b}{m(y)}\Phi_\kappa^j(y)\varphi_k^j(y)\,\mathrm{d}y.$$

Eliminating B_κ^{ij} from (19) leads to a set of linear homogeneous algebraic equations for A_k^{ij}. This set has a non-trivial solution only if its determinant is equal to zero. Writing down the

determinant, we get the secular equation for the energy E^{tr}. Determining the energy spectrum from the secular equation, we then calculate coefficients A_k^{ij} and B_κ^{ij} from (19). Finally, a substitution of A_k^{ij} and B_κ^{ij}, respectively, in the expansions (6) and (7) gives the wavefunction $\Psi(x, y)$.

In our calculations the sum over k is restricted to $k < k_{\text{max}}$, where k_{max} is defined from the condition $\hbar^2 k_{\text{max}}^2 / 2m_w = 4V_b$. We have found that this restriction allows us to calculate the complete discrete energy spectrum ($E^{\text{tr}} < V_b$) with a good accuracy regardless of the number of the quantum wires N. Taking $5V_b$ instead of $4V_b$ in previous equality, we obtain a correction to the energy spectrum of less than 1%. It should be noted, that unlike k_{max}, the number of terms in the expansions (6) and (7) rises with increasing N, due to the aforementioned relation $2R = NL + 6L$. In a single GaAs/Ga$_{0.63}$Al$_{0.37}$As quantum wire, according to the above presented equalities for R and k_{max}, it is sufficient to take 20 terms in (6) and (7), in order to calculate all 10 discrete energy levels. In a lattice with six QWWs (the period $L = 15$ nm) the number of terms is taken to be 40, in order to find all 60 discrete energy levels.

3. Infinite lattice

In this section we consider an infinite lattice of rectangular quantum wires. The method already described for the single quantum wire and for a finite lattice cannot be applied straightforwardly for the infinite lattice, because of infinite number of terms with $k < k_{max}$ in (6) and (7). Therefore, we use the expansions for $\Psi(x, y)$ similar to those of (6) and (7) with the x and y coordinates transposed with respect to each other. In these expansions $\varphi_k(x)$ and $\Phi_\kappa(x)$ are the functions (defined by (9), (11) and (14)) of a single wire extended along the x-axis.

In the case of an infinite lattice, the effective barrier potential $V^{\text{eff}}(x, y)$ and the band mass $m(x, y)$ are periodic functions of the y coordinate, i.e. $V^{\text{eff}}(x, y + L) = V^{\text{eff}}(x, y)$ and $m(x, y+L) = m(x, y)$. Hence, due to the translation symmetry of the system, the wavefunction $\Psi(x, y)$ obeys the relation [29]

$$\Psi(x, y + L) = \exp(\mathrm{i}k_y L)\Psi(x, y) \tag{20}$$

where k_y is a quantum number satisfying the inequalities $-\pi/L \leqslant k_y \leqslant \pi/L$. It is worth noting that k_y can be interpreted as a quasi-wavenumber of the motion of an electron or a hole along the y-axis.

The solution of the Schrödinger equation (3), which satisfies the relation (20), and which is defined within the period $|y| \leqslant L/2$, has the form

$$\Psi(x, y) = \begin{cases} \displaystyle\sum_\kappa \Phi_\kappa(x)[B_\kappa^* g(y - L_y/2 + L) \\ \quad - B_\kappa g(y + L_y/2)\mathrm{e}^{-\mathrm{i}k_y L}] & -L/2 \leqslant y < -L_y/2 \\ \displaystyle\sum_k \varphi_k(x)[A_k^s F_k^s(y) + \mathrm{i}A_k^a F_k^a(y)] & |y| \leqslant L_y/2 \\ \displaystyle\sum_\kappa \Phi_\kappa(x)[B_\kappa^* g(y - L_y/2)\,\mathrm{e}^{\mathrm{i}k_y L} \\ \quad - B_\kappa g(y + L_y/2 - L)] & L_y/2 < y \leqslant L/2 \end{cases} \tag{21}$$

where

$$g(t) = \frac{\sinh(\xi_\kappa t)}{\sinh(\xi_\kappa(L - L_y))}$$

$F_k^i(y)$ and ξ_κ were defined in the previous section; B_κ^* is a complex conjugated value of B_κ. In a general case, the coefficients B_κ as well as the wavefunction $\Psi(x, y)$ have complex values, while the coefficients A_k^s and A_k^a get real values, as shown below.
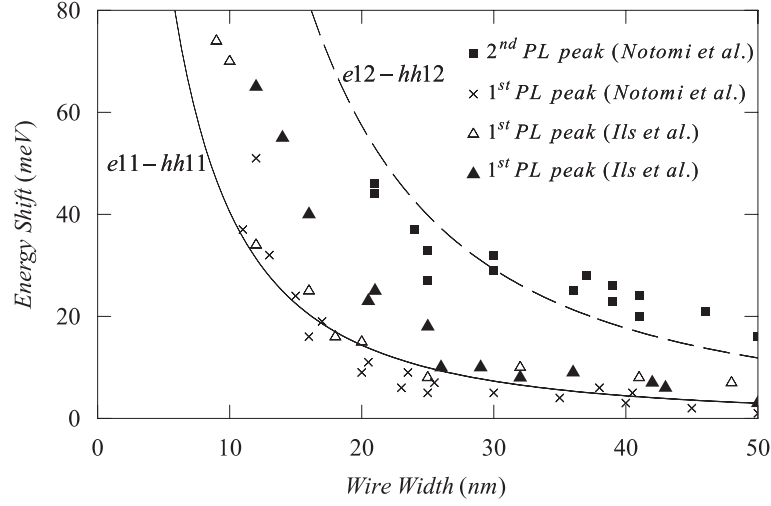
Figure 2. Energy shift in photoluminescence spectra versus the width L_x of the rectangular $Ga_{0.47}In_{0.53}As$/ InP quantum wire ($L_y = 5$ nm). The energy shift is calculated with respect to the photoluminescence spectrum of the $Ga_{0.47}In_{0.53}As$ slab of thickness 5 nm.

Requiring the continuity of the wavefunction $\Psi(x, y)$ together with its derivative divided by the band mass at the lines $y = -L_y/2$ and $y = L_y/2$ we obtain the following set of linear algebraic equations for the coefficients A_k^s, A_k^a and B_κ:

$$\operatorname{Re} B_\kappa = \sum_k d_{k\kappa} A_k^s F_k^s(L_y/2) \qquad \operatorname{Im} B_\kappa = \sum_k d_{k\kappa} A_k^a F_k^a(L_y/2)$$

$$\xi_\kappa \frac{\operatorname{Re} B_\kappa (\cosh(\xi_\kappa(L - L_y)) - \cos(k_y L)) - \operatorname{Im} B_\kappa \sin(k_y L)}{\sinh(\xi_\kappa(L - L_y))} = \sum_k D_{k\kappa} A_k^s F_k^{s\prime}(L_y/2)$$

$$\xi_\kappa \frac{\operatorname{Re} B_\kappa \sin(k_y L) - \operatorname{Im} B_\kappa (\cosh(\xi_\kappa(L - L_y)) + \cos(k_y L))}{\sinh(\xi_\kappa(L - L_y))} = \sum_k D_{k\kappa} A_k^a F_k^{a\prime}(L_y/2) \qquad (22)$$

where $\operatorname{Re} B_\kappa$ and $\operatorname{Im} B_\kappa$ are the real and imaginary parts of B_κ. On the basis of (22), substituting $\operatorname{Re} B_\kappa$ and $\operatorname{Im} B_\kappa$ from the first two equations into the last two, we obtain a set of linear homogeneous algebraic equations for A_k^s and A_k^a. Notice, that the equations for A_k^s and A_k^a contain real terms only, and hence the coefficients A_k^s and A_k^a are real, too. Equating the determinant of the obtained set of equations to zero, we get a secular equation for the energy E^{tr}. Solving this secular equation, we find the energy $E^{\mathrm{tr}}(k_y)$ as a function of k_y. Then, after calculating the coefficients A_k^s, A_k^a and B_κ from (22), we can find the wavefunction $\Psi_{k_y}(x, y)$ for certain k_y using expressions (21). If A_k^s and A_k^a form a solution for a quantum state with a quasi-wavenumber k_y, then A_k^s and $-A_k^a$ are a solution for a quantum state with a quasi-wavenumber $-k_y$, due to the invariance of (22) with respect to the simultaneous substitutions $k_y \rightarrow -k_y$ and $A_k^a \rightarrow -A_k^a$. On the other hand, these substitutions are equivalent to the replacement $\Psi_{k_y}(x, y) \rightarrow \Psi_{k_y}^*(x, y)$. Therefore, the wavefunction obeys the property $\Psi_{-k_y}(x, y) \equiv \Psi_{k_y}^*(x, y)$. All terms of the Schrödinger equation (3) are real, hence $\Psi_{k_y}(x, y)$ and $\Psi_{k_y}^*(x, y)$ satisfy the Schrödinger equation with the same energy $E^{\mathrm{tr}}(k_y)$. Consequently, the quantum states with quasi-wavenumbers k_y and $-k_y$ have the same energy, i.e. $E^{\mathrm{tr}}(k_y) = E^{\mathrm{tr}}(-k_y)$.
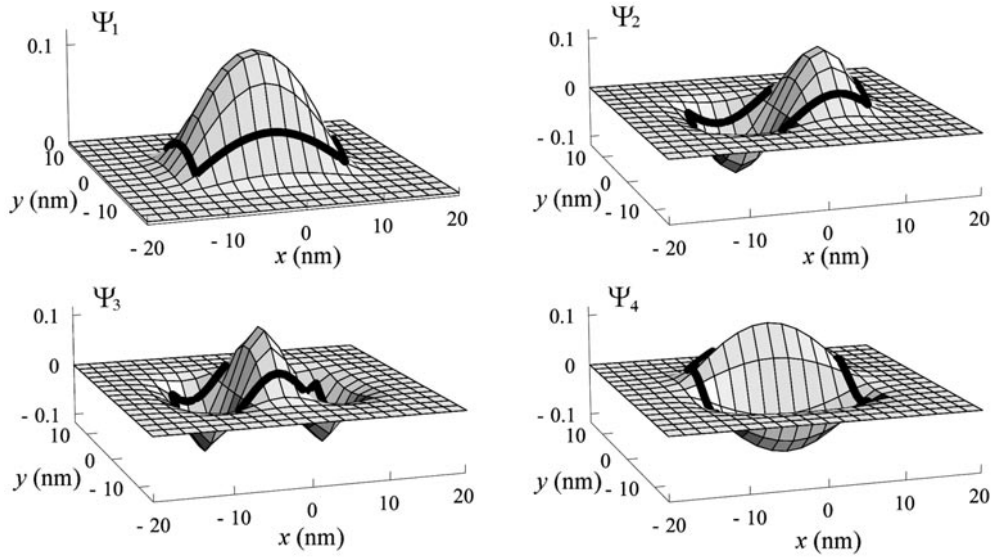
Figure 3. Wavefunctions of four quantum states ($l = 1, \ldots, 4$) for an electron in the GaAs/Ga$_{0.63}$Al$_{0.37}$As single quantum wire with the dimensions $L_x = 20$ nm and $L_y = 10$ nm. $E_1^{tr} = 42.270$ meV; $E_2^{tr} = 73.079$ meV; $E_3^{tr} = 123.86$ meV; $E_4^{tr} = 135.22$ meV.

4. Results of calculation and discussion

In order to justify the accuracy of the method, first of all we carry out the calculations for the single rectangular GaAs/Ga$_{0.63}$Al$_{0.37}$As and Ga$_{0.47}$In$_{0.53}$As/InP quantum wires. For those QWWs the lowest energy levels were found in [15] and [16], respectively. The material parameters have the following values for the GaAs/Ga$_{0.63}$Al$_{0.37}$As structure [16]

- conduction electron: $m_w = 0.0665m_e$, $m_b = 0.0858m_e$, $V_b = 276$ meV
- light hole: $m_w = 0.0905m_e$, $m_b = 0.1107m_e$, $V_b = 184$ meV
- heavy hole: $m_w = 0.3774m_e$, $m_b = 0.3865m_e$, $V_b = 184$ meV

and for the Ga$_{0.47}$In$_{0.53}$As/InP structure [16]

- conduction electron: $m_w = 0.042m_e$, $m_b = 0.079m_e$, $V_b = 240$ meV
- heavy hole: $m_w = 0.47m_e$, $m_b = 0.61m_e$, $V_b = 370.6$ meV.

Our analytical calculation reproduces the values of the lowest eigenenergies obtained in [15, 16]. Also we find the energy shift in the Ga$_{0.47}$In$_{0.53}$As/InP quantum wire with respect to a Ga$_{0.47}$In$_{0.53}$As slab of the same thickness. For the calculations we take $L_y = 5$ nm, while L_x is varied from 5 to 50 nm. In figure 2 the results of these calculations are plotted together with experimental data from [23, 24]. Comparing our theoretical results with experiments of [23, 24] we should point out a considerable scatter in experimental data. This could be the result of geometrical and compositional inhomogeneities of the wire, which grow with weakening confinement. The results of measurements are considerably altered even for different samples (see figure 2, the first PL peaks for two samples are marked as empty and full triangles). Taking this into account, the agreement of the experimental and theoretical data can be stated as good for the ground-state energy and fair for the first excited state. Having checked the accuracy of our method, we carried out the following calculations.
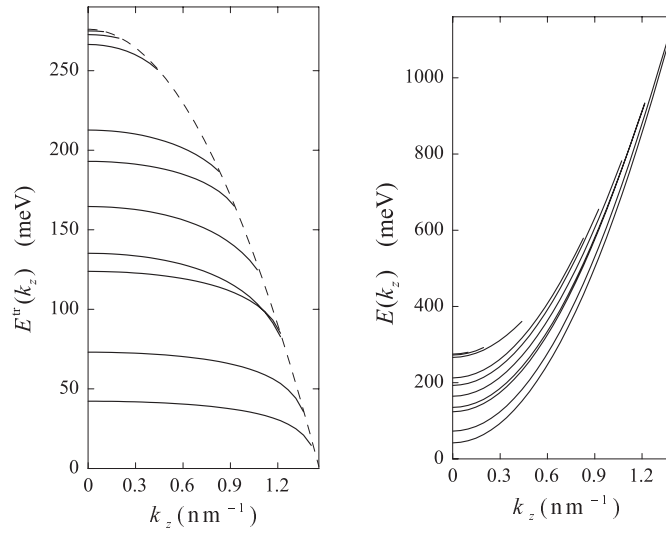
Figure 4. Energy of the transverse motion (left-hand panel) and full energy (right-hand panel) of an electron in a single QWW versus the wavenumber k_z. A dashed curve indicates the effective potential V^{eff}. The curves for energy are broken off as $E^{\text{tr}}(k_z)$ becomes higher than V^{eff}.

(1) For the single rectangular GaAs/Ga$_{0.63}$Al$_{0.37}$As quantum wire with dimensions $L_x = 20$ nm and $L_y = 10$ nm, all ten discrete energy levels E_l^{tr} ($l = 1, \ldots, 10$) and the corresponding wavefunctions $\Psi_l(x, y)$ are calculated. In figure 3 the wavefunctions ($k_z = 0$) of the four lowest quantum states are plotted as 3D-graphs. The bold curve in these graphs is a projection of the quantum wire border on the surface. It can be seen from figure 3 that the higher quantum states penetrate into the barrier region more strongly than the lower ones. As shown below, the penetration substantially influences the miniband width of an infinite lattice.

The wavefunctions $\Psi_l(x, y)$ with $l = 1, \ldots, 7$ and 10 have a rather simple structure and can be classified by introducing quantum numbers n_x and n_y, which indicate the number of half-waves along the x- and y-axes, respectively. Using such a classification, we can indicate the following pairs of (n_x, n_y): (1, 1); (2, 1); (3, 1); (1, 2); (2, 2); (4, 1); (3, 2) for the quantum states with $l = 1$ to 7, correspondingly, and $n_x = 4$, $n_y = 2$ for the state with $l = 10$. The remaining wavefunctions $\Psi_8(x, y)$ and $\Psi_9(x, y)$ cannot be classified in this way. If one increases the height of the barrier V_b, the discrete quantum states of a single quantum wire tend to the well known quantum states (n_x, n_y) in a rectangular quantum wire with infinite height of the barrier. In such a limit, the quantum states with $l = 8$ and 9 tend to the quantum states with $n_x = 1$, $n_y = 3$ and $n_x = 5$, $n_y = 1$, respectively.

(2) In figure 4 the energies E_l^{tr} ($l = 1, \ldots, 10$) are plotted as a function of k_z. If the band masses in the quantum wire and in the barrier were the same, then the total energy E would depend on k_z as a parabolic function and the energy E_l^{tr} would be a constant. In figure 4, we emphasize a deviation of the above energies from the parabolic dependence due to different band masses ($m_b > m_w$), while the electron's dispersion law in the well and barrier materials is parabolic. As k_z increases, the height of the effective potential V^{eff} decreases in this case. Hence, when the energy E_l^{tr} is close to the height of the effective potential, this deviation becomes significant. For higher quantum states, the deviation from the parabolic dependence becomes appreciable at smaller values of k_z as compared with those for lower quantum states. The diminishing of E_l^{tr} with increasing k_z can be explained by the penetration

$k_z = 0$
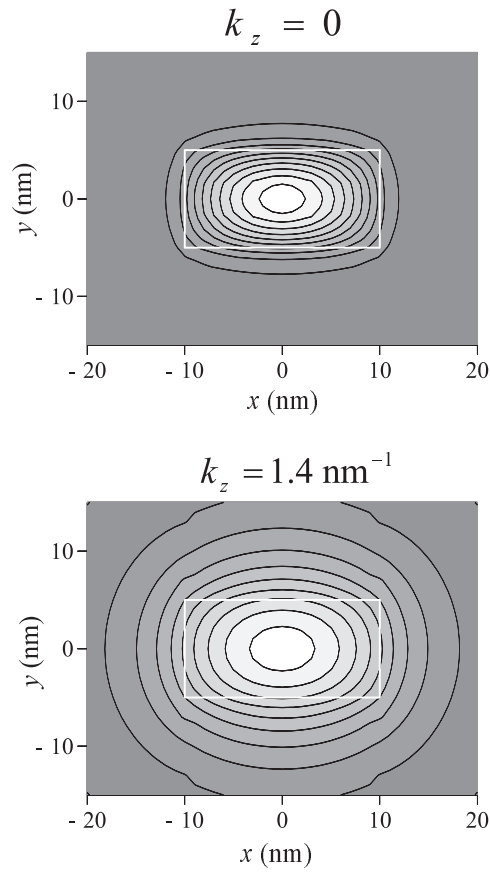

$k_z = 1.4 \text{ nm}^{-1}$

Figure 5. Penetration of the ground-state wavefunction into the barrier region for an electron moving along the quantum wire axis. $E_1^{\text{tr}}(0) = E_1(0) = 42.27 \text{ meV}$; $E_1^{\text{tr}}(1.4 \text{ nm}^{-1}) = 16.46 \text{ meV}$, $E_1(1.4 \text{ nm}^{-1}) = 1140 \text{ meV}$.

of the wavefunction in the barrier region, where the band mass is heavier than that inside the quantum wire. Consequently, the penetration of the wavefunction in the barrier is deeper for higher k_z (see figure 5). So, due to a deep penetration of the wavefunction $\Psi_4(x, y)$ $(n_x = 1, n_y = 2)$ in the barrier in comparison with that of $\Psi_3(x, y)$ $(n_x = 3, n_y = 1)$, at large $k_z \approx 1.1 \text{ nm}^{-1}$ the energy level E_4 becomes lower than E_3.

(3) Next we consider results of calculations for the lattice with six rectangular quantum wires. The quantum wires are arranged in one plane and parallel to each other. In the plane the width is $L_x = 20 \text{ nm}$ and the period is $L = 15 \text{ nm}$. The thickness of a QWW is $L_y = 10 \text{ nm}$. Three specific cases with the edge barrier potentials $V_0 = V_b$, $2V_b$ and $V_b/2$ are investigated in detail for quantum states with $k_z = 0$. Hereafter we take $m_0 = m_b$.

Each quantum state of a single quantum wire transforms into six quantum states in the lattice with six QWWs. This process can be imagined as a split of a six-fold degenerate energy level into six energy levels of the lattice. If one increases the distance between the quantum wires $L - L_y$ to infinity, the value of this split tends to zero, and the wavefunction in each quantum wire coincides with the wavefunction Ψ_l^{single} of a single quantum wire. Therefore, we can classify the quantum states in a finite lattice by two quantum numbers l and p, where

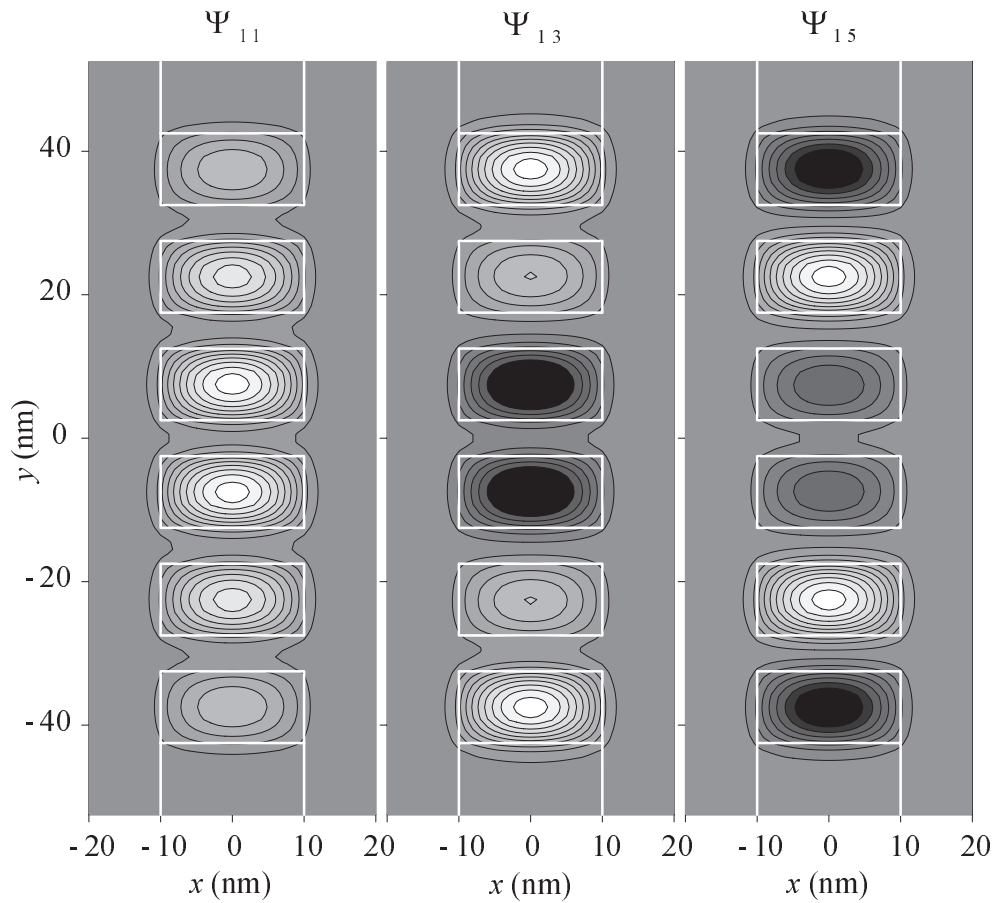**Figure 6.** Electron wavefunctions ($l = 1$, $p = 1, 3, 5$) in the finite lattice with six quantum wires ($V_0 = V_b$). $E_{11}^{\text{tr}} = 41.622$ meV; $E_{13}^{\text{tr}} = 42.101$ meV; $E_{15}^{\text{tr}} = 42.712$ meV.

l corresponds to the quantum number of the energy level in a single quantum wire (taking the limit $L - L_y \to \infty$) and p labels the energy levels with the same l. For a fixed l, three quantum states with $p = 1, 3, 5$ have symmetrical wavefunctions along the y-axis, while another three quantum states $p = 2, 4, 6$ have antisymmetrical wavefunctions. Here we represent only the quantum states with symmetrical wavefunctions.

First, we discuss the case $V_0 = V_b$, for which the contour plots of the electron wavefunctions with $l = 1$ and $p = 1, 3, 5$ are shown in figure 6. A modulation of the wavefunction Ψ_l^{single} is seen to occur along the y-axis. Therefore, the wavefunction of a quantum state in the lattice can be approximately written as a product $\Psi_{lp} = f_p \Psi_l^{\text{single}}$ of an envelope function f_p and of the wavefunction Ψ_l^{single} in a single quantum wire. For the wavefunction Ψ_{11}, the envelope function has a maximum in the middle ($y = 0$) of the lattice and monotonously decreases along the positive and negative directions of the y-axis. The wavefunctions Ψ_{13} and Ψ_{15} are modulated by the envelope functions with three and five half-waves along the y-axis.

A variation of the barrier height V_0 at the lattice edges substantially changes the wavefunctions of an electron or a hole in the finite lattice. For two particular cases $V_0 = 2V_b$
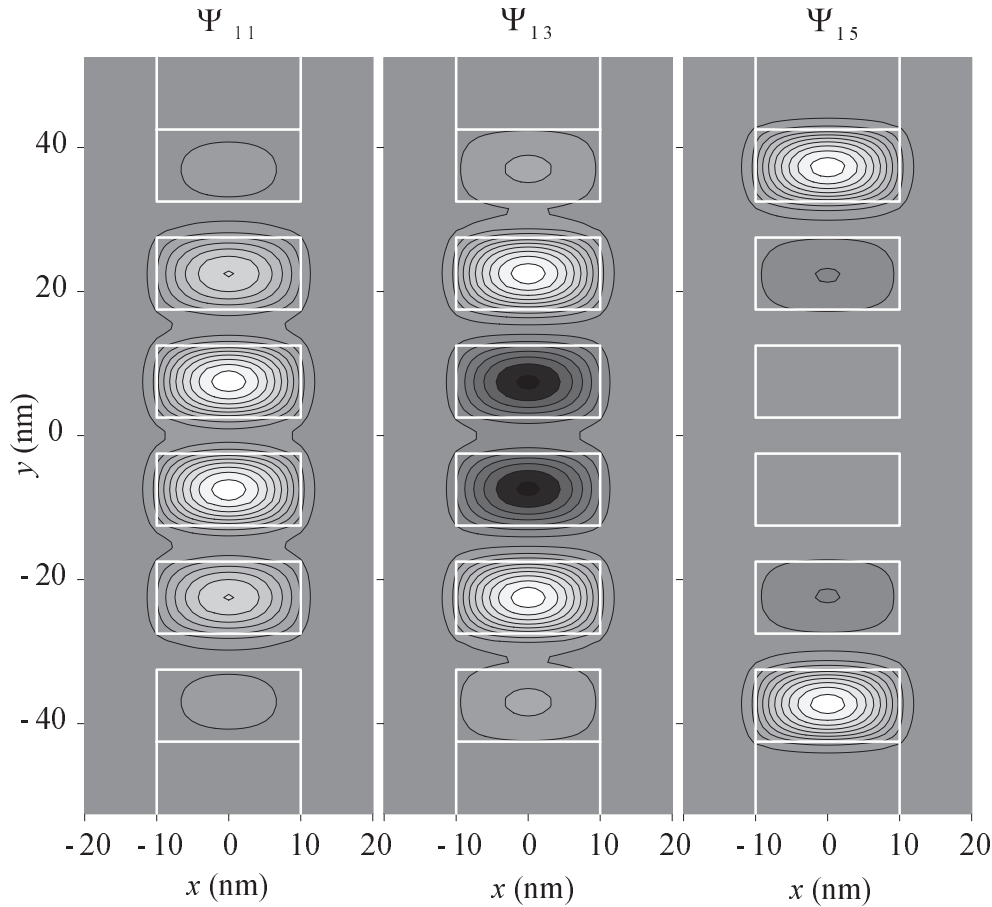
Figure 7. Electron wavefunctions ($l = 1$, $p = 1, 3, 5$) in the finite lattice with six quantum wires ($V_0 = 2V_b$). $E_{11}^{tr} = 41.673$ meV; $E_{13}^{tr} = 42.437$ meV; $E_{15}^{tr} = 44.810$ meV.

and $V_b/2$, the electron wavefunctions ($l = 1$, $p = 1, 3, 5$) are represented in figures 7 and 8, respectively. In figure 7 the wavefunctions with $p = 1$ and 3 have a similar shape to those for $V_0 = V_b$, but they are expelled from the lattice edges. On the contrary, the wavefunction with $p = 5$ is strongly localized near the outermost wires and penetrates into the lattice only by a length of one period. Hereafter, we refer to them as to *edge quantum states*. The same effect happens for the case $V_0 = V_b/2$ (figure 8), where the wavefunction with $p = 1$ is localized near the lattice edges, while the wavefunctions with $p = 3, 5$ are appreciable in the middle four QWWs only. The wavefunctions of the edge quantum states for the case $V_0 < V_b$ penetrate deeper in the barrier than those for $V_0 > V_b$. In the case $V_0 = V_b/2$, the edge quantum state possesses the lowest energy E_{11}, while in the opposite case $V_0 = 2V_b$ the highest energy level E_{15} corresponds to the edge quantum state. It should be noted that the same picture can be seen for the antisymmetrical quantum states. The antisymmetrical wavefunctions with indices $p = 2$ and $p = 6$ correspond to the edge quantum states in the cases $V_0 < V_b$ and $V_0 > V_b$, respectively.

(4) The dependence of the electron energy levels ($l = 1$, $p = 1, \ldots, 6$) on the height of the edge barrier V_0 is plotted in figure 9. When $V_0 = V_b$, all six energy levels lie inside the first
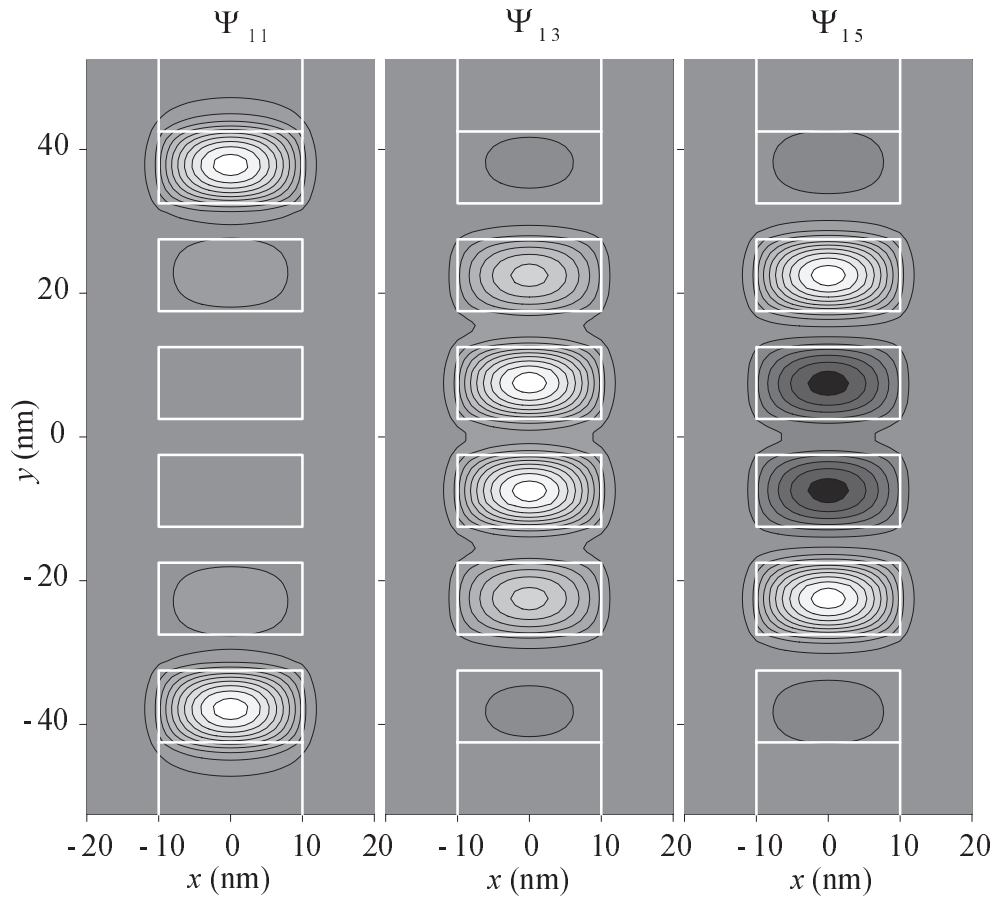
Figure 8. Electron wavefunctions ($l = 1$, $p = 1, 3, 5$) in the finite lattice with six quantum wires ($V_0 = V_b/2$). $E_{11}^{\text{tr}} = 39.078$ meV; $E_{13}^{\text{tr}} = 41.697$ meV; $E_{15}^{\text{tr}} = 42.506$ meV.

miniband of an infinite lattice (the miniband energy structure of an infinite lattice is discussed below). If one increases the ratio V_0/V_b, the two highest energy levels, which correspond to the symmetrical and antisymmetrical edge quantum states, go up off the miniband. In the opposite case of small ratios $V_0/V_b < 1$, the two lowest energy levels go down off the miniband edge. In both cases, the two energy levels of the edge quantum states become very close to each other. The rest of the four energy levels always lie inside the miniband. It is worth mentioning that, due to such a degeneracy of the energy levels of the edge quantum states, a linear combination of the corresponding symmetrical and antisymmetrical wavefunctions is an approximate solution of the Schrödinger equation (3). Consequently, we can construct the wavefunctions, which are localized only at one edge of the lattice as $\Psi_{l\pm} = (\Psi_{l5} \pm \Psi_{l6})/\sqrt{2}$ for $V_0 > V_b$ and $\Psi_{l\pm} = (\Psi_{l1} \pm \Psi_{l2})/\sqrt{2}$ for $V_0 < V_b$. One of the wavefunctions $\Psi_{l\pm}$ corresponds to the edge quantum state in a semi-infinite lattice (a lattice with an infinite number of QWWs and one edge).

(5) Similarly to a superlattice, the infinite lattice of QWWs has a miniband energy structure. Each miniband with the energy $E_l(k_y)$ originates from the energy level E_l of a single quantum wire. In figure 10 the miniband energy $E_l(k_y)$ is shown for the infinite lattice with the period
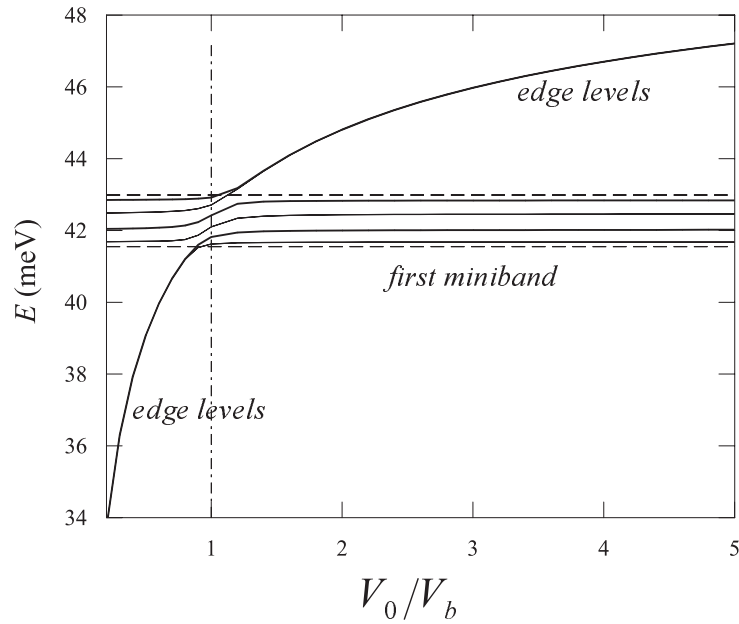
Figure 9. Energy levels ($l = 1$, $p = 1, \ldots, 6$) of an electron in the finite lattice with six quantum wires versus the edge barrier potential V_0.

$L = 15$ nm. The infinite lattice consists of the rectangular quantum wires with the dimensions $L_x = 20$ nm and $L_y = 10$ nm. Corresponding to ten discrete energy levels in a single quantum wire, the infinite lattice has 10 minibands. The wavenumber k_y is restricted to the interval $-\pi/L \leqslant k_y \leqslant \pi/L$, since the energy $E_l(k_y)$ is a periodic function of k_y with the period $2\pi/L$. The formation of a miniband can be imagined as a splitting of an infinitely degenerate energy level of a single quantum wire. It is important to note, that an energy level of a single QWW lies exactly in the middle of the corresponding miniband. In the minibands $l = 1, 2, 3, 6, 8, 9$, the energy $E_l(k_y)$ has a minimum at $k_y = 0$, while in the minibands $l = 4, 5, 7, 10$ at $k_y = 0$, $E_l(k_y)$ is maximal. The quantum states $l = 1, 2, 3, 6$ in a single quantum wire are classified by the quantum number $n_y = 1$, and, correspondingly, the quantum states $l = 4, 5, 7, 10$ have $n_y = 2$. Since the quantum states with $n_y = 2$ penetrate into the barrier deeper than the quantum states with $n_y = 1$, the corresponding minibands labelled by $l = 4, 5, 7, 10$ are wider than those with $l = 1, 2, 3, 6$.

In a general case, the wavefunction of an electron or a hole in an infinite lattice acquires complex values. According to (20), in an infinite lattice the wavefunction is exactly represented as a product of the envelope function $e^{ik_y y}$ and a wavefunction of a single quantum wire.

5. Conclusions

A theoretical method is developed, which allows an insight to be obtained into the electronic properties of a single quantum well wire with a rectangular cross section, as well as of the finite and infinite planar lattices of such wires. Using this method, the electron and hole discrete energy levels are calculated and the obtained electron–hole pair energies are found to be in good agreement with the experimental data. The dependence of the electron energy $E(k_z)$ and the wavefunction on the wavenumber k_z was investigated. Due to different band masses inside
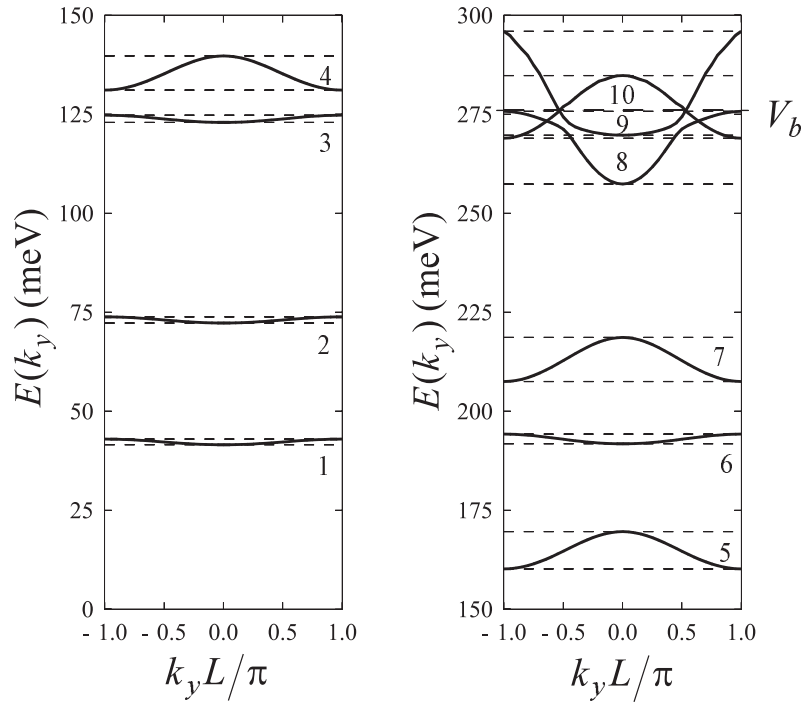
Figure 10. Energy minibands of an electron in an infinite lattice ($k_z = 0$).

and outside the quantum wire ($m_b > m_w$), the electron wavefunction penetrates deeper into the barrier as the wavenumber k_z rises, and, consequently, $E(k_z)$ is a non-parabolic function of k_z. In this way, the ratio of effective masses in the well and in the barrier influences the electron transport along the QWW axis.

The energy levels and the wavefunctions of the electron quantum states in the finite lattice of six QWWs were investigated. The quantum states in a finite lattice are formed from those of a single quantum wire. Therefore, the energy spectrum of a finite lattice can be interpreted as a split of the energy levels of a single QWW. Consequently, the wavefunction in each quantum wire is modulated by an envelope function along the entire lattice. When the height of the external potential barrier differs from that of the internal one (which is between the quantum wires), the edge quantum states occur. The wavefunction of an edge quantum state is localized near the lattice edges, while the wavefunctions of the rest quantum states are expelled from the edges. Each energy level of the edge quantum states has a very close neighbour, which is characterized by the opposite parity with respect to inversion of the lattice axis.

The energy spectrum of an infinite lattice has a miniband structure. Each miniband corresponds to a discrete energy level in a single quantum wire.

Acknowledgments

References

[1] Asada M, Miyamoto Y and Suematsu Y 1985 *Japan. J. Appl. Phys.* **24** L95
[2] Tsukamoto S, Nagamune Y, Nishioka M and Arakawa Y 1993 *Appl. Phys. Lett.* **62** 49
[3] Nakajima Y, Takahashi Y, Horiguchi S, Iwadate K, Namatsu H, Kirihara K and Tabe M 1994 *Appl. Phys. Lett.* **65** 2834
[4] Dneprovskii V, Zhukov E, Karavanskii V, Poborchii V and Salamatina I 1998 *Superlattices Microstruct.* **23** 1217
[5] Grundmann M, Christen J, Joschko M, Stier O, Bimberg D and Kapon E 1994 *Semicond. Sci. Technol.* **9** 1939
[6] Vouilloz F, Oberli D Y, Dupertuis M-A, Gustafsson A, Reinhardt F and Kapon E 1998 *Phys. Rev.* B **57** 12 378
[7] Langbein W, Gislason H and Hvam J M 1996 *Phys. Rev.* B **54** 14 595
[8] Pescetalli S, Carlo A D and Lugli P 1997 *Phys. Rev.* B **56** 1668
[9] Stier O and Bimberg D 1997 *Phys. Rev.* B **55** 7726
[10] Bryant G W 1984 *Phys. Rev.* B **29** 6632
[11] Chuu D S, Hsiao C M and Mei W N 1992 *Phys. Rev.* B **46** 3898
[12] Brown J W and Spector H N 1986 *J. Appl. Phys.* **59** 1179
[13] Bryant G W 1985 *Phys. Rev.* B **31** 7812
[14] Pokatilov E P, Fomin V M, Balaban S N, Klimin S N and Devreese J T 1998 *Phys. Status Solidi* b **210** 879
[15] Shertzer J and Ram-Mohan L R 1990 *Phys. Rev.* B **41** 9994
[16] Gangopadhyay S and Nag B R 1996 *Phys. Status Solidi* b **195** 123
[17] Citrin D S and Chang Y-Ch 1989 *Phys. Rev.* B **40** 5507
[18] Vasilopoulos P, Warmenbol P, Peeters F M, and Devreese J T 1989 *Phys. Rev.* B **40** 1810
[19] Chüller Ch 1998 *Physica* E **3** 121
[20] Osorio F A P, Degani M H and Hipolito O 1988 *Phys. Rev.* B **37** 1402
[21] Weber G, Schulz P A and Oliveira L E 1988 *Phys. Rev.* B **38** 2179
[22] Moukhliss S, Fliyou M and Es-Sbai N 1998 *Phys. Status Solidi* b **206** 593
[23] Notomi M, Naganuma M, Nishida T, Tamamura T, Iwamura H, Nojima S and Okamoto M 1991 *Appl. Phys. Lett.* **58** 720
[24] Ils P, Michel M, Forchel A, Gyuro I, Klenk M and Zielinski E 1994 *Appl. Phys. Lett.* **64** 496
[25] Cibert J, Petroff P M, Dolan G J, Peatron S J, Gossard A C and English G H 1986 *Appl. Phys. Lett.* **49** 1275
[26] Sogawa T, Ando H, Ando S and Kanbe H 1997 *Phys. Rev.* B **56** 1958
[27] Notomi M, Nojima S, Okamoto M, Iwamura H, Tamamura T, Hammersberg J and Weman H 1995 *Phys. Rev.* B **52** 11 073
[28] Notomi M, Hammersberg J, Weman H, Nojima S, Siguira H, Okamoto M, Tamamura T and Potemski M 1995 *Phys. Rev.* B **52** 11 147
[29] Kittel C 1967 *Quantum Theory of Solids* (New York: Wiley)